www.czasopisma.pan.pl PAN www.journals.pan.pl
Opto-Electronics Review 27 (2019) 329–333

Contents lists available at ScienceDirect

Opto-Electronics Review

journal homepage: http://www.journals.elsevier.com/opto-electronics review

Full Length Article

The operation of THz quantum cascade laser in the region of negative differential resistance

R.A. Khabibullin[a,b], N.V. Shchavruk[a], D.S. Ponomarev[a,b], D.V. Ushakov[c], A.A. Afonenko[c], K.V. Maremyanin[d], O.Yu. Volkov[e], V.V. Pavlovskiy[e], A.A. Dubinov[d,*]

[a] *V.G. Mokerov Institute of Ultra High Frequency Semiconductor Electronics of RAS, Moscow, Russia*
[b] *Center for Photonics and 2D Materials, Moscow Institute of Physics and Technology, Dolgoprudny, Russia*
[c] *Belarusian State University, Minsk, Belarus*
[d] *Institute for Physics of Microstructures of RAS, Nizhny Novgorod, Russia*
[e] *Institute of Radio-Engineering and Electronics of RAS, Moscow, Russia*

ARTICLE INFO

Article history:
Received 1 October 2019
Received in revised form 7 November 2019
Accepted 7 November 2019
Available online 25 November 2019

Keywords:
Quantum-cascade laser
THz region
Resonant-phonon design
Negative differential resistivity

ABSTRACT

We investigate the light-current-voltage characteristics and emission spectra of 2.3 THz quantum cascade laser operating in the negative differential resistance (NDR) region. It was shown that the formation of electric field domains (EFDs) leads to a large number of discontinuities on the current-voltage and the total optical power on current characteristics. Measurements of emission spectra at different current (before the NDR region and in the NDR region) shows that the formation of EFDs results in decrease of the output intensity, but does not influence on Fabry-Perot multi-mode structure of THz QCL. The developed theoretical model predicts the formation of EFDs in the NDR region and qualitatively explain the experimental results.

1. Introduction

Electron transport in quantum cascade lasers (QCLs) is based on a combination of resonant tunneling and intersubband scattering in multiple quantum wells (MQWs), which may be called as sequential resonant-tunneling. The first experimental observation of the sequential resonant-tunneling is demonstrated for MQWs superlattice with an operating bias point outside the region of negative differential resistance (NDR) [1]. Using this approach and adding to the structure a doped digitally graded alloy ("injector"), the first QCL is demonstrated [2]. Thus, avoiding NDR in operating dynamic range is a common design concept for QCL active regions in order to prevent instabilities.

The vast majority of QCL designs are based on the assumption of homogeneous distribution of applied electric field along the entire active region. At the same time, the resonant coupling between quantized states (for example, between injector level and upper laser level) is expected to result in appearance of NDR, which is confirmed experimentally in many works [3–5]. Moreover, electric potential distribution inside operating QCLs was measured thanks to the scanning voltage microscopy at a cryogenic temperature [6]. It was shown that electric potential might be simultaneously spatial nonuniform and temporally unstable, which corresponds to the formation of electrical field domains (EFD).

In this work, we investigate the light-current-voltage (L- I-V) characteristics and emission spectra of THz QCL operating in the NDR region. The performed calculations qualitatively explain the experimental results.

2. Fabrication of THz QCL and measurement procedures

We have designed THz QCL with active module based on four QWs GaAs/$Al_{0.15}Ga_{0.85}As$ with resonant-phonon (RP) depopulation scheme. The maximum gain of the proposed design is realized under RP conditions at a wavelength of 130 μm which corresponds to the frequency of 2.3 THz. The laser structure was grown by molecular beam epitaxy with a 12 μm active region thickness. The layer thicknesses (in nm) of one cascade, starting from the injector barrier, are as follows: 5.7/**8.2**/3.1/**7.1**/4.2/**16.1**/3.4/**9.6**, where the thicknesses of GaAs QWs are shown in bold. The central part of the wide QWs is doped with a Si impurity with a layer concentration of 3.1×10^{10} cm^{-2}. In the structure under study, the active QCL region lies between the contact layers with a dopant concentration of 5×10^{18} cm^{-3}. The thickness of the lower n^+-GaAs contact layer

* Corresponding author.
E-mail address: sanya@ipmras.ru (A.A. Dubinov).

https://doi.org/10.1016/j.opelre.2019.11.002
1230-3402/

was of 50 nm and the thickness of the upper n^+-GaAs contact layer was of 800 nm.

For fabrication of THz QCL with Au-Au double metal waveguide we used the conventional processing described in Refs. [7] and [8]. The fabricated ridge structures with a 1.6 and 2.6 mm cavity length and a 100 μm cavity width were mounted onto copper C-mounts.

The current–voltage (I-V) characteristics of the fabricated THz QCL structures were investigated at T =4.2 K in the pulsed mode. THz QCL on an insert was placed in an STG-40 transport helium Dewar vessel. The structures were fed using an original electron switch based on an IRF 9510 field-effect transistor. The rectangular driving voltage pulses with a length of 10–20 μs and a repetition rate of 100–1000 Hz were formed by a G5-56 generator.

The emission spectra were measured using an evacuated Bruker Vertex80v Fourier spectrometer in the step scan mode [9]. THz QCL with a sapphire hyperhemispherical lens was mounted on the cold finger of the cryostat employing nitrogen vapor evacuation to cool the laser at 54 K. The laser radiation was detected by a room temperature pyroelectric detector built into the spectrometer. The experiments were carried out without nitrogen purge of the gap between cryostat windows and spectrometer; therefore, a part of the THz QCL radiation was absorbed by water vapor in the surrounding atmosphere. Estimated THz QCL power was about 1 mW.

3. The theoretical model of THz QCL

The calculation of the THz QCL characteristics starts with the determination of the integral characteristics of one cascade depending on the applied voltage. For this, the Schrödinger equation was solved and the energy levels and wave functions were determined [10]. Next, the procedure of localization of wave functions was carried out [11]. After this we calculated the matrix elements of dipole transitions, the probabilities of scattering by optical phonons and impurities, as well as the probability of electron-electron scattering in the approximation of thermodynamic equilibrium in subbands. The probability of tunnel junctions was calculated in the random phase approximation with Lorentz line contours. Level populations were found from a system of balanced equations for one cascade of structure. The electron leakage times from a localized level to the continuum states were estimated from the amplitudes of the wave functions in the continuum region similarly to the lifetimes of optical modes in the cavity [12]. The need for introducing leakages into the continuum in the analysis is due to the use of a limited basis of wave functions that does not take into account the entire set of continuum states. The gain spectrum was determined similarly to Refs. [13] and [14] taking into account the contribution of non-resonant transitions [11]. The many-particle effects of electron-electron interaction were taken into account as in Ref. [15]. The calculations of the coefficient of total losses, including losses on the gold claddings of a double metal waveguide, on the resonator mirrors and on free charge carriers, as well as losses from absorption on optical phonons, were carried out in the same way as in Ref. [16]. The current – voltage characteristics and the dependence of the integrated radiation intensity on the current were calculated on the basis of the distributed model presented in Ref. [11]. Contact resistance was considered equal to 3 ohms. Given the large reflection coefficient (R ~ 0.9) of terahertz radiation on a laser facet, the mirrors loss coefficient did not exceed 1 cm^{-1}.

For the proposed design of THz QCL with active module based on four QWs GaAs/$Al_{0.15}Ga_{0.85}As$ the calculated conduction band diagram, wave functions, energy levels, and dipole matrix elements are shown in Fig. 1. At the operation bias point V_1 = 48 meV per module, injector levels 1 and upper laser level 5 are aligned which leads to resonant tunneling of electrons. Transitions of electron from upper laser level 5 to lower laser levels 3 and 4 is accompanied by THz photon emission. Finally, electrons in the lower lasing levels relax to level 1 through fast electron–longitudinal phonon scattering. This process then repeats in subsequent modules.

The maximum gain G_{max} = 41 cm^{-1} at 54 K is realized for applied bias on one cascade V_1 = 48 meV per module (see Fig. 2). Dependence of the current density through the cascade on the V_1 shows that the maximum gain is achieved on the descending branch of the I–V characteristics, which corresponds to formation of NDR region. It should be noted that in the lasing mode when photon densities S>0 the NDR region shifts toward higher voltages (see Fig. 2, dotted lines) and gain maximum decreases.

4. Experimental results and discussions

Fig. 3 shows the experimental current-voltage (I–V) characteristics and voltage dependence of the radiation intensity (L–V) for THz QCL with a 1.6 mm cavity length. Current leakages into the continuum are small and weakly affect the output characteristics,

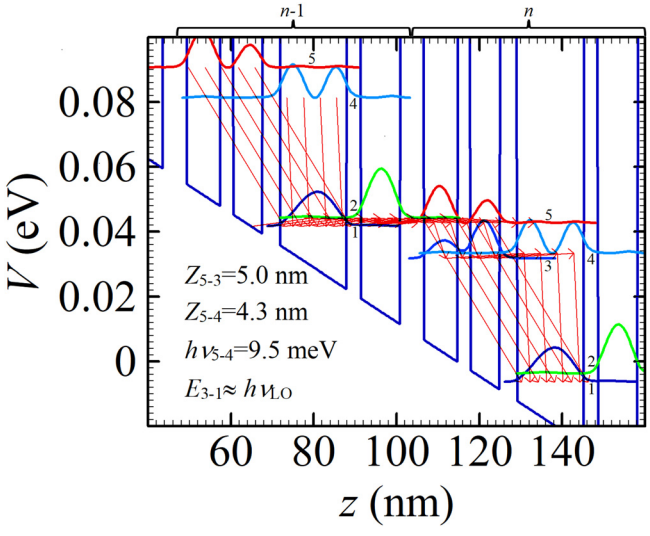

Fig. 1. Conduction band diagram of the GaAs/$Al_{0.15}Ga_{0.85}As$ four well QCL, wave functions, energy levels and dipole matrix elements at a bias of V_1 = 48 mV/period and T = 54 K where the gain is maximal on frequency of 2.3 THz. The red arrows show the intensity of the current flow through the levels.

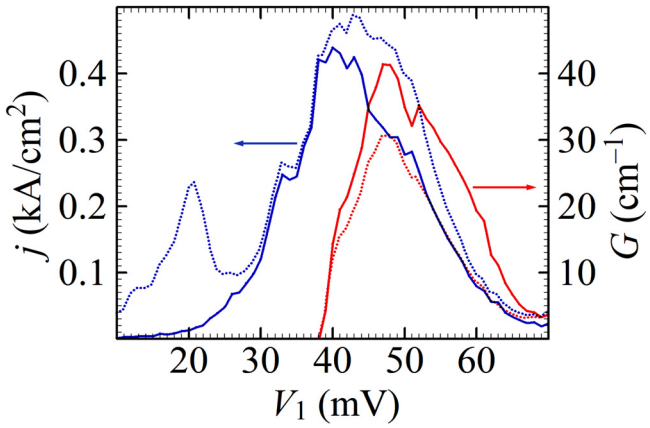

Fig. 2. Dependences of the current density through the cascade j (blue) and the gain G (red) at a frequency of 2.3 THz on the applied bias V_1 at 54 K for photon densities 0 (solid line) and 1.8 10^{15} cm^{-3} (dotted line).

and the electric field is almost uniform throughout the structure on the increasing branch of the I–V characteristics. The lasing threshold occurs at J_{th} =785 mA (voltage – 10.48 V). The nonmonotonic behavior of L–V characteristics around 11 V is observed as what we associate with mode hopping. The peak power of THz QCL is achieved at a current of 886 mA (voltage – 11.3 V) which corresponds to the alignment of the injector level and upper laser level. A weak emission power (about 5 % of the peak value) is observed above 14.5 V.

A pronounced NDR region appears at voltages higher than 11.3 V. In this region, the I–V characteristics has a large number of discontinuities. We suppose that such electric instabilities associated with the field inhomogeneity across the active region. Our calculations show that on the increasing branch of the I–V characteristics, the electric field is almost uniform over the entire structure. On the decline branch of the I–V characteristics, the dynamic EFDs arise in the structure. For the described structure the formation of sections across the active region with distinctly different electric field under the bias higher than 9 V (see Fig. 4). The field strength in the domain grows until it reaches the next positive portion of the I–V characteristics. In this case, the gain is realized only in a part of the structure outside the region of a strong field, and the radiation power decreases. Due to the instability of the domains, jumps on the I–V and L-I characteristics of the laser occur (see Fig. 3). Furthermore, the discontinuities of the L-I characteristics are correlated to the discontinuities in the I–V characteristics. Similar voltage profile and L-I characteristics in QCLs was observed experimentally in Refs. [5] and [6].

Fig. 5 shows the emission spectra of THz QCL with a 2.6 mm cavity length operating at different current (before the NDR region and in the NDR region). In measured at 54 K spectra there are several equidistant spectral lines corresponding to the longitudinal Fabry-Perot modes with Δf =16 GHz. In a current biasing range from 1.376 A to 1.451 A (see Fig. 5A) the lasing spectra consist of two strong spectral modes at 2.251 and 2.267 THz. With increasing current, additional modes appear at frequencies 2.283, 2.990 and 2.315 THz with a gradual transfer of energy from low-frequency to high-frequency modes. This effect is associated with a shift of the G_{max} to high frequencies, as well as a shift in the minimum loss to the high-frequency region [16].

In the NDR region (see Fig. 5B) we measure the emission spectra of THz QCL in current biasing range from 1.475 to 1.541 A. The lasing spectra consist of two strong spectral modes of 2.990 and 2.315 THz, which we observe in current range before NDR region.

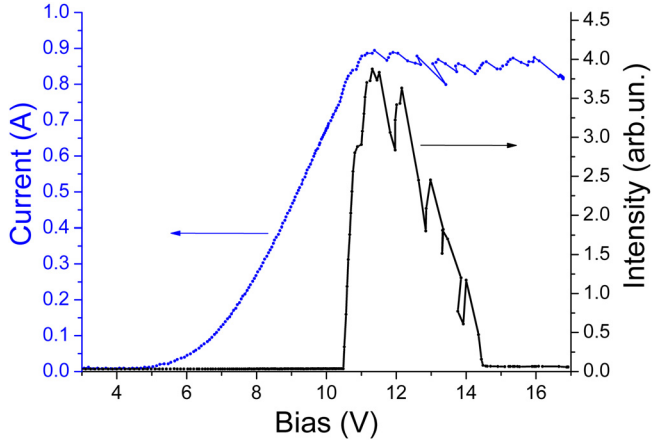

Fig. 3. L–I–V characteristic of fabricated THz QCL measured at 4.2 K in pulse mode with pulse width of 10 μs and repetition rate of 1 kHz for voltage biasing.

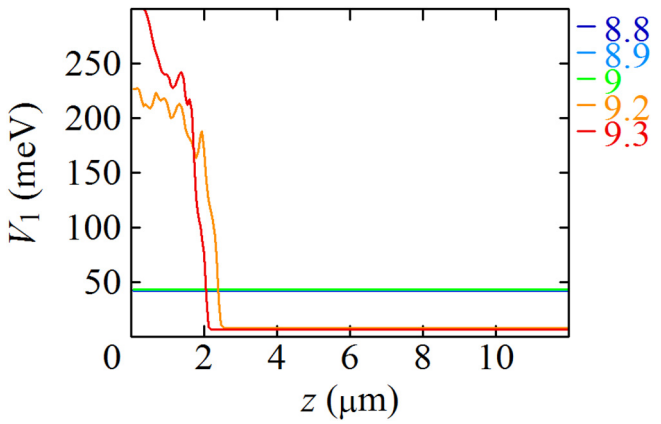

Fig. 4. Voltage profile across the active region of a THz QCL under different bias. The numbers indicate the voltage (in V) on the structure without the account of the contacts and external resistances.

Hence, the formation of EFDs does not influence on Fabry-Perot multi-mode structure of THz QCL. At currents above 1.523 A the intensity of spectral lines start to decrease sharply which can be associated with two reasons: 1) misalignment of the electron levels (in particular between lower laser level and extractor level) at high bias; 2) formation of EFDs with distinctly different electric field.

5. Conclusions

We investigate the light-current-voltage characteristics and emission spectra of a 2.3 THz quantum cascade laser with RP design operating in the NDR region. The I–V and L–V characteristics have a large number of discontinuities above 11.3 V bias voltage due to the formation of multiple sections across the active region with distinctly different electric field (electric field domains - EFDs) in this NDR region. The performed calculations show that on the decline branch of the I–V characteristics, the dynamic EFDs arise in the structure. It was experimentally shown that the formation of EFDs does not influence on Fabry-Perot multi-mode structure, but it affects of the output power of THz QCL.

Authors statements

Authors confirm that there are no known conflicts of interest, other than directly indicated in the manuscript.

Authors confirm that if the study described in the manuscript of the work involved animals or humans as subjects, then these studies were performed according to applicable standards as directly described in the manuscript.

Authors confirm that, if the study described in the manuscript of the work involved animals or humans as subjects, then written informed consent was obtained from all human participants involved in the study as directly described in the manuscript.

Acknowledgements

This study was supported by the Russian Foundation for Basic Research, project no. 18-52-00011 Bel_a, and the Belarussian Republican Foundation for Basic Research, project no. F18R-107. The fabrication of THz QCLs was supported by the Russian Science Foundation, grant no. 18-19-00493.

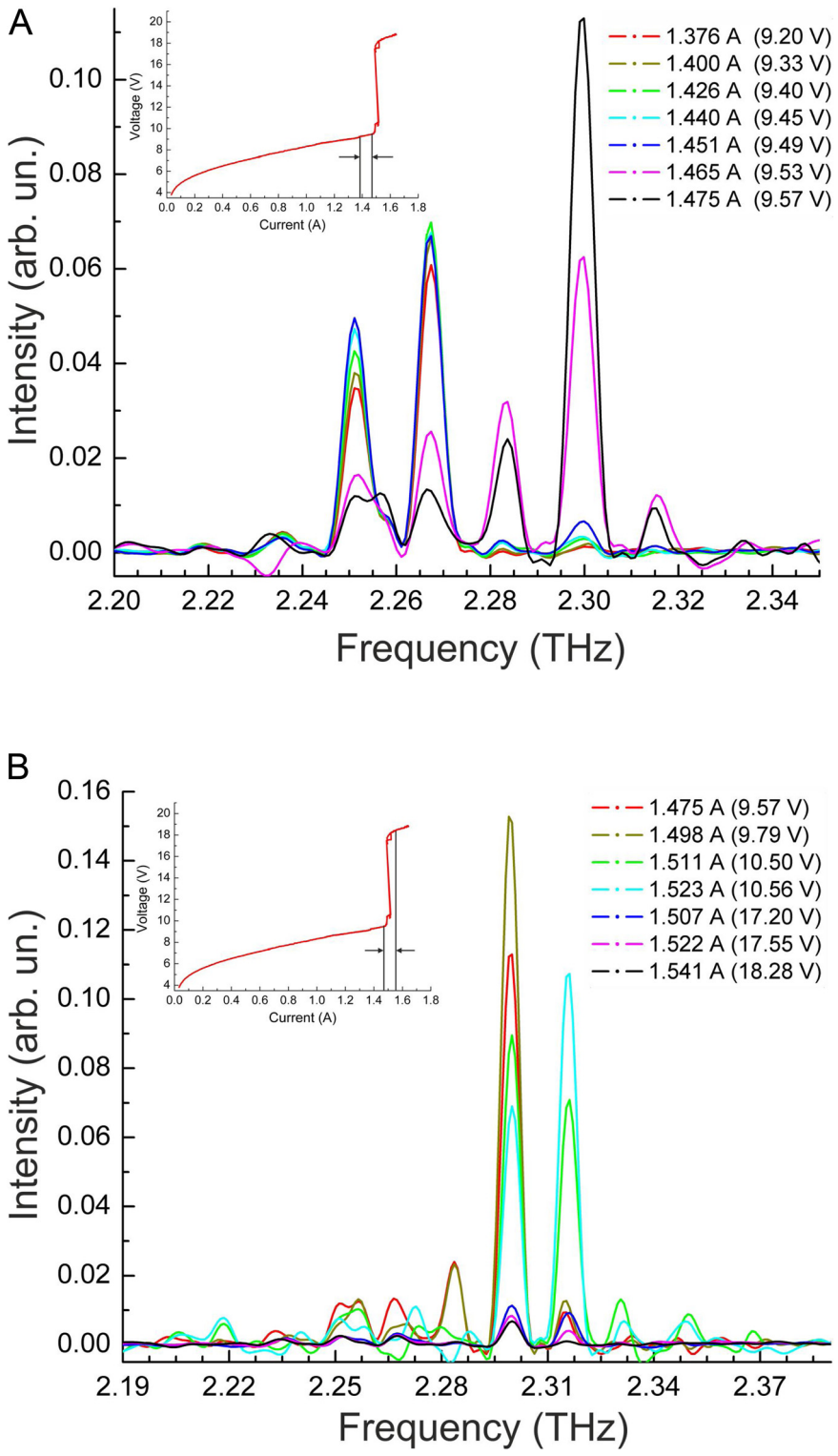

Fig. 5. Measured at 54 K emission spectra of THz QCL at different current: *a*, before the NDR and *b*, in the NDR region. I–V characteristic for current biasing with a marked current region for spectral measurements is shown in the inset.

References

[1] F. Capasso, K. Mohammed, A.Y. Cho, Sequential resonant tunneling through a multiquantum well superlattice, Appl. Phys. Lett. 48 (7) (1986) 478.
[2] J. Faist, F. Capasso, D.L. Sivco, C. Sirtori, A.L. Hutchinson, A.Y. Cho, Quantum cascade laser, Science 264 (1994) 553.
[3] S.L. Lu, L. Schrottke, R. Hey, H. Kostial, H.T. Grahn, Negative differential conductance and current bistability in undoped GaAs/(Al,Ga)As quantum-cascade structures, J. Appl. Phys. 97 (2005), 024511.
[4] A. Albo, Q. Hu, J. Reno, Room temperature negative differential resistance in terahertz quantum cascade laser structures, Appl. Phys. Lett. 109 (2016), 081102.
[5] M. Wienold, L. Schrottke, M. Giehler, R. Hey, H.T. Grahn, Nonlinear transport in quantum-cascade lasers: the role of electric-field domain formation for the laser characteristics, J. Appl. Phys. 109 (2011), 073112.
[6] R.S. Dhar, S.G. Razavipour, E. Dupont, C. Xu, S. Laframboise, Z. Wasilewski, Q. Hu, D. Ban, Direct nanoscale imaging of evolving electric field domains in quantum structures, Sci. Rep. 4 (2014) 7183.

[7] R.A. Khabibullin, N.V. Shchavruk, A.Y. Pavlov, D.S. Ponomarev, K.N. Tomosh, R.R. Galiev, P.P. Maltsev, A.E. Zhukov, G.E. Cirlin, F.I. Zubov, Z.I. Alferov, Fabrication of a terahertz quantum-cascade laser with a double metal waveguide based on multilayer GaAs/AlGaAs heterostructures, Semiconductors 50 (10) (2016) 1377.
[8] A.V. Ikonnikov, K.V. Marem'yanin, S.V. Morozov, V.I. Gavrilenko, A.Yu. Pavlov, N.V. Shchavruk, R.A. Khabibullin, R.R. Reznik, G.E. Cirlin, F.I. Zubov, A.E. Zhukov, Zh.I. Alferov, Terahertz radiation generation in multilayer quantum-cascade heterostructures, Tech. Phys. Lett. 43 (4) (2017) 358.
[9] O.Yu. Volkov, I.N. Dyuzhikov, M.V. Logunov, S.A. Nikitov, V.V. Pavlovskii, N.V. Shchavruk, A.Yu. Pavlov, R.A. Khabibullin, Analysis of terahertz radiation spectra in multilayer GaAs/AlGaAs heterostructures, J. Commun. Technol. Electron. 63 (9) (2018) 1042.
[10] D.V. Ushakov, I.S. Manak, Energy and emission characteristics of superlattice quantum-cascade structures, Opt. Spectrosc. 104 (5) (2008) 767.
[11] D.V. Ushakov, A.A. Afonenko, A.A. Dubinov, V.I. Gavrilenko, O.Yu. Volkov, N.V. Shchavruk, D.S. Ponomarev, R.A. Khabibullin, Balance equations method for simulation of terahertz quantum cascade lasers using the wave functions basis with reduced dipole moments of tunnel-coupled states, Quantum Electron. 49 (2019) 913–918.
[12] A.A. Afonenko, V.Ya. Aleshkin, A.A. Dubinov, Efficiency of vertical emission from a semiconductor laser waveguide with a diffraction grating, Semiconductors 48 (1) (2014) 89.
[13] V.B. Gorfinkel, S. Luryi, B. Gelmont, Theory of gain spectra for quantum cascade lasers and temperature dependence of their characteristics at low and moderate carrier concentrations, Quantum Electron. 32 (1996), 1995.
[14] D.V. Ushakov, V.K. Kononenko, I.S. Manak, Calculation of gain and luminescence spectra of quantum-cascade laser structures taking into account asymmetric emission line broadening, Quantum Electron. 40 (2010) 195.
[15] A.N. Drozd, A.A. Afonenko, Effect of Coulomb interaction of electrons on the intersubband emission lineshape in quantum wells, J. Appl. Specrtosc. 74 (5) (2007) 710.
[16] D.V. Ushakov, A.A. Afonenko, A.A. Dubinov, V.I. Gavrilenko, I.S. Vasil'evskii, N.V. Shchavruk, D.S. Ponomarev, R.A. Khabibullin, Mode loss spectra in THz quantum-cascade lasers with gold-and silver-based double metal waveguides, Quantum Electron.
48 (2018) 1005.